Title: Sandwiched Droplet Actuated by Marangoni Force in a Hele-Shaw Cell

Authors

Vi-Vie Ng

Department of Mechanical Engineering, University of Canterbury, Private Bag 4800, Christchurch, 8140, New Zealand

e-mail: vivienne.ng@pg.canterbury.ac.nz

Mathieu Sellier (**Corresponding Author**)

Department of Mechanical Engineering, University of Canterbury, Private Bag 4800, Christchurch, 8140, New Zealand

Phone: (+64) (3) 364 2987 ext. 7248

e-mail: mathieu.sellier@canterbury.ac.nz

Volker Nock

Department of Electrical and Computer Engineering, University of Canterbury, Private Bag 4800, Christchurch, 8140, New Zealand

e-mail: volker.nock@canterbury.ac.nz

Abstract

We present a novel method of actuating a microliter droplet held within a Hele-Shaw cell by means of surface tension gradient or Marangoni effect. A food color droplet is first injected within the gap formed by the parallel plates to produce a cylindrical droplet, followed by a lateral injection of a lower surface tension droplet. Our results showed the actuation of the food color droplet, for various droplet volumes and viscosities. Analytical studies on the effect of contact angle on distance traveled are presented. Numerical values of Marangoni force showed good agreement with analytical values. Mathematical analysis showed the surface tension difference required for actuation, and how the surface tension changes as a function of angular position on the droplet.

Keywords

Hele-Shaw, Droplet actuation, Surface tension, Marangoni

Introduction

A Hele-Shaw cell is commonly used to model two-phase flow confined within a small gap. The device comprises of two parallel plates separated by a distance much smaller than the characteristic length of the plates, such that the liquid flow in between the plates is laminar. It has been used to model studies in a wide range of areas, namely oil recovery [1], CO_2 geological storage [2], transport in capillary blood vessels [3], droplets in microfluidics [4], semiconductor chip packaging [5], as well as photovoltaic cell production [6].

Experiments with vertical [2, 7, 8] as well as tilted [9] Hele-Shaw cells have been carried out where, in the latter case, bubbles of various shapes rising in a surrounding liquid was reported. Works pertaining to droplets in a Hele-Shaw cell, to date, typically involve a droplet suspended in an aqueous phase. Amselem et al. [10] studied the behavior of oil droplets subjected to various flow rates of the surrounding glycerol-water solution. Huerre et al. [11] correlated the motion of a droplet with the lubrication film between a droplet and a wall. The morphology of these resulting pancake droplets have been numerically studied by Brun et al. [12] and Oswald et al.[13]. Experimental works pertaining to solutal Marangoni in a Hele-Shaw cell have been reported, such as the mass transfer of liquid [14] and the coalescence of drops [15]. Thermocapillary-driven Marangoni flow of droplets and air bubbles [16, 17] has also been investigated using the Hele-Shaw cell [18, 19].

When a microliter droplet is formed in between the parallel plates without an external flow, it takes on the shape of a cylinder. Though theoretical studies of a cylindrical droplet subjected to an external flow [20] and a surface tension gradient [21] have been published, none have reported the

experimental observation of an actuating cylindrical droplet in a Hele-Shaw cell, to the best of our knowledge. Hence, the original contributions of this paper are to:

- demonstrate droplet actuation in a Hele-Shaw cell by the solutal Marangoni effect which occurs when two miscible droplets are juxtaposed in the cell;
- present a new analytical and numerical methodology to quantify the resultant Marangoni and dissipative forces acting on the droplet;
- estimate the mass transport between the two interacting droplets.

The motivation behind this work is to present a mechanism that may be a potential alternative to the transport of reagent droplets in enclosed microfluidic devices [22–24]. It is important for the devices to be enclosed, particularly when the droplets under test might be hazardous to the user and environment [25]. Our proposed method of droplet actuation, which does not rely on external sources of power, eliminates the risk of excessive pressure build up and can be suited for portable devices.

Materials and methods

We used pre-cleaned plain rectangular microscope glass slides (Thermo Fisher Scientific, Australia) measuring 75 x 25 x 1 mm as the parallel plates of our Hele-Shaw cell. A commercial double-sided foam tape of thickness 0.5 mm was used to create the spacing: four square pieces measuring ~ 5 x 5 mm were cut and attached at the four corners to separate the two glass plates. To ensure that the plates were parallel, we observed the injected droplet to confirm that it was stationary. A deviation from parallelism would induce motion. Also, the cell was placed on a glass table that was leveled using a bubble level gauge each time prior to an experiment. Otherwise, a

tilted surface would cause the droplet to move. Using a glass syringe (Hamilton, USA), a droplet of commercial blue food color (Hansells, New Zealand), used as received, was injected perpendicular to the length of the Hele-Shaw cell. Following that, an equal volume of ethanol (EtOH) was injected in the same manner from a lateral distance ~1.5 mm relative to the stationary blue droplet. A video of the experiment can be viewed at https://youtu.be/HP8WhU1U05w. The experiment was performed in a controlled environment, where the cell was also assembled: 21 °C +/- 1 ^{o}C and 50% humidity. Using a digital single-lens reflex (DSLR) camera (Canon EOS 760D), the experiment was recorded at 50 frames per second. By overlaying a frame chosen for a particular time of interest on top of the frame showing the initial position of the droplet, a measurement line was drawn from the center of one droplet to the other. Based on the pixel-to-actual length scale set on these measurements, the actual length of the line drawn was then obtained. All image processing were performed using Image J [26].

Analytical model

The motion of a droplet in a Hele-Shaw cell is representative of the force balance between the force arising from surface tension gradient or Marangoni force, F_σ, as well as the viscous resistive force, F_r (see Fig. 1(a)). From Newton's second law,

$$m\frac{dV}{dt} = F_\sigma - F_r, \tag{1}$$

where V is the traveling velocity of the droplet in the *x*-direction.

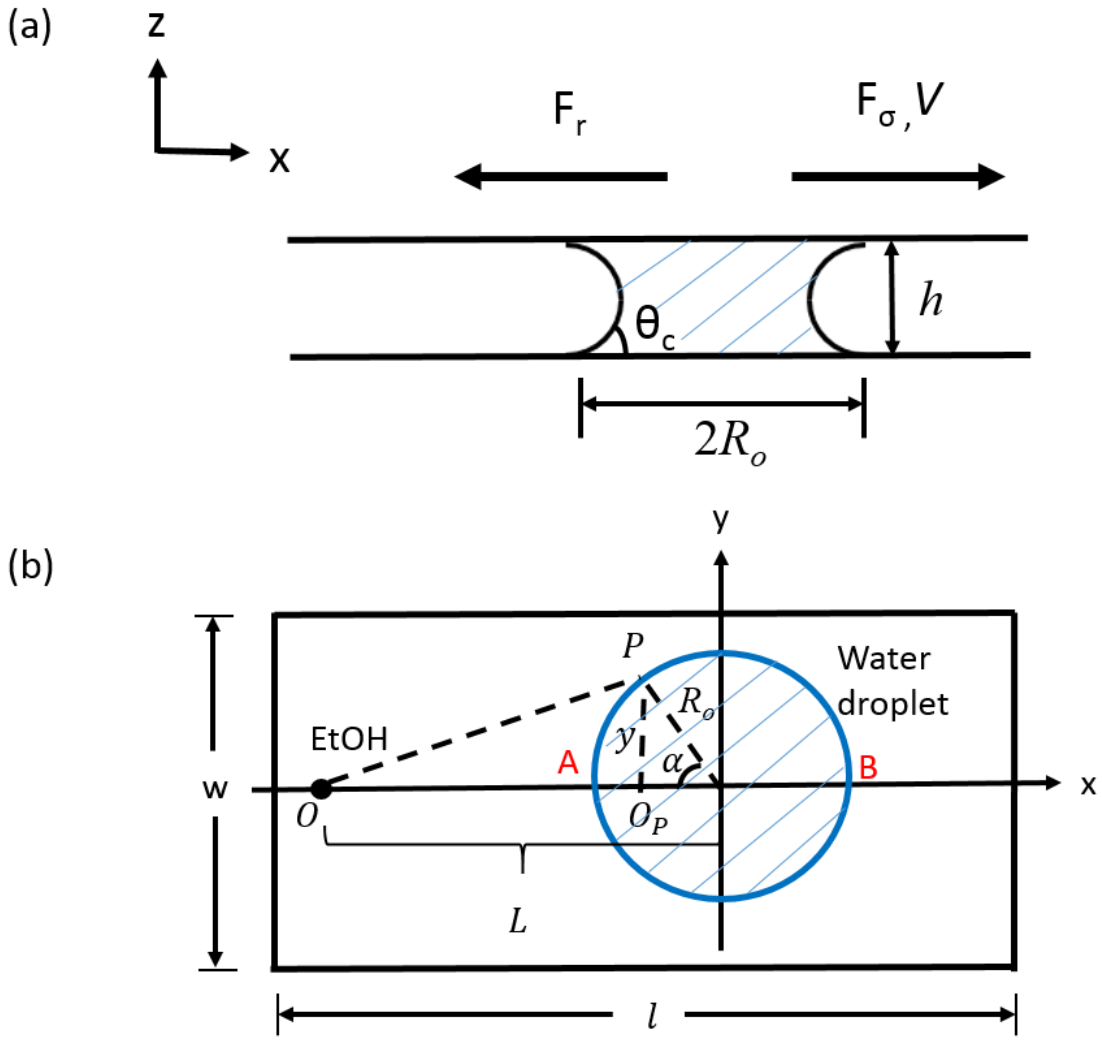

Fig. 1 An illustration depicting (a) the side view and (b) the top view of a food color droplet with contact angle θ_c in a rectangular Hele-Shaw cell of length l, width w, and height h. Pictures are not drawn to scale.

Following the analogy from Ahmed et al. [27], along with the inclusion of two circular footprints for our droplet in a Hele-Shaw cell, the viscous resistive force, F_r can be expressed as

$$F_r = 2\int_0^{R_o} \tau_w (2\pi r)\, dr, \tag{2}$$

where τ_w is the wall shear stress, given by

$$\tau_w = \frac{6\mu V}{h}. \tag{3}$$

R_o represents the radius of the droplet and h the height of the Hele-Shaw gap. Substitution of Eq. (3) into Eq. (2) yields

$$F_r = \frac{12\pi R_o^2 \mu V}{h}. \tag{4}$$

The Marangoni force, F_σ can be expressed as a function of angular surface tension, $\sigma(\alpha)$ as follows:

$$F_\sigma = 4R_o \cos\theta_c \int_0^{\pi} \cos\alpha \cdot \sigma(\alpha)\, d\alpha, \tag{5}$$

where θ_c represents the equilibrium/Young contact angle. For convenience, we shall assume a trigonometric distribution of the surface tension such that

$$\sigma(\alpha) = \sigma_A + (\sigma_B - \sigma_A)\sin\frac{\alpha}{2}. \tag{6}$$

Therefore, solving Eq. (6) by substitution of Eq. (5) yields

$$F_\sigma = \frac{8}{3}R_o\cos\theta_c\,(\sigma_B - \sigma_A). \tag{7}$$

In addition, the concentration of EtOH vapor in air can be modeled using the diffusion of an EtOH point source in two-dimension theory [28]. The pertinent equation is given by

$$C(x, y, t) = \frac{M}{4\pi hDt}e^{-\frac{(x^2+y^2)}{4Dt}}, \tag{8}$$

where we assume a uniform diffusion coefficient, D. M represents the mass of ethanol and h, the height of the cell gap is included to depict a three-dimensional case. A schematic of an EtOH point source relative to a water droplet in a Hele-Shaw cell is illustrated in Fig. 1(b). The distance from the EtOH point source, O to an angular position P, α degrees from the x-axis, is expressed as

$$\overrightarrow{OP} = \overrightarrow{OO_P} + \overrightarrow{O_PP} \tag{9}$$

which, upon further expansion becomes

$$\overrightarrow{OP} = (L - R_o \cos \alpha)\vec{x} + R_o \sin \alpha \vec{y}, \tag{10}$$

where L is the center-to-center distance between the EtOH point source and the water droplet, and R_o the radius of the water droplet. Substituting the expression in Eq. (10) into Eq. (8), we obtain an expression for the angular EtOH vapor concentration:

$$C(L, R_o, \alpha, t) = \frac{M}{4\pi hDt} e^{-\frac{\left(L^2 + 2R_o^2 - 2LR_o \cos \alpha\right)}{4Dt}}. \tag{11}$$

Numerical model

Our objective is not to directly model the experiment, but rather, to obtain the viscous resistance force, F_r in order to estimate the Marangoni force, F_σ. First, a constant body force is imposed to obtain the terminal velocity. At the terminal velocity, the body force equals the viscous resistive force [29], thus allowing for the calculation of the viscous resistive force. Using various body force values, a relationship between viscous resistive force and terminal velocity is obtained. Therefore, the viscous resistive forces corresponding to experimental velocities can be obtained and subsequently used to calculate the Marangoni force, F_σ. A similar methodology has been reported by Karpitschka et al. [30], where the interaction force between two droplets sliding down a soft solid due to gravitational force was determined from their relative velocities.

To model a droplet in a Hele-Shaw cell, we first constructed a half-cylinder according to the dimensions of a 3 μl droplet measured from our experiment, detailed in the next section. Instead

of modeling a full cylinder, we save computational time by modeling a half-cylinder with symmetry imposed on the center cross-section parallel to the *xz*-plane.

Using the Laminar Two-Phase Flow Moving Mesh physics in COMSOL, the velocity field **u** is solved through the following Navier-Stokes equation:

$$\rho \frac{\partial \mathbf{u}}{\partial t} + \rho(\mathbf{u} \cdot \nabla)\mathbf{u} = \nabla \cdot [-p\mathbf{I} + \mu(\nabla \mathbf{u} + (\nabla \mathbf{u})^T)] + \boldsymbol{F}, \tag{12}$$

and

$$\frac{\partial \rho}{\partial t} + \nabla \cdot (\rho \mathbf{u}) = 0, \tag{13}$$

where μ is the dynamic viscosity and $\boldsymbol{F}$ is a body force imposed in the *x*-direction. The momentum equation as shown in Eq. (12) is a non-linear convection-diffusion equation that would be unstable if discretized using the Galerkin finite element method. As such, streamline diffusion is included for stabilization. Isotropic diffusion with a default tuning parameter, $\delta_{id} = 0.25$ is included to dampen the effects of oscillations. To model the solid walls on the top and bottom of the droplet, we impose a boundary condition that specifies a frictional force:

$$\boldsymbol{F}_{fr} = -\frac{\mu}{\beta}\mathbf{u}, \tag{14}$$

where $\beta = 0.2 * m$ represents the Navier slip length for a mesh element size of m. This boundary condition, used together with Prescribed Displacement perpendicular to the wall, enables the liquid-air interface to move along the wall. At the three-phase boundary, the Navier slip condition, in addition to the wall-fluid interface that specifies a contact angle of 45°, ensures that the droplet maintains a consistent contact angle. The half-cylinder model built was discretized to 20,788 domain elements, 2404 boundary elements and 159 edge elements. Winslow smoothing is chosen such that the mesh is smoothly deformed given the boundary conditions. Linear P1 elements are chosen for both the velocity and pressure components. The air-liquid interface is modeled under the External Fluid Interface node through the following equation:

$$\mathbf{n}\cdot\mathbf{T} = -p_{ext}\mathbf{n} + \sigma(\nabla_t \cdot \mathbf{n})\mathbf{n} - \nabla_t\sigma, \tag{15}$$

where the external pressure, p_{ext} is set to 0. The surface tension, σ is specified as 0.072 N/m to represent the surface tension of water.

Results and discussion

I. Experimental

A blue food color droplet was injected in between two parallel rectangular plates of length *l* and width *w*, separated by a height, *h*. The stationary droplet formed was circular with concave menisci due to surface tension (see Fig. 1(a)). The contact angle measured was ~ 45°. The shape of the blue droplet transitioned from a circle to a slight ellipse upon the injection of EtOH (see $t = 1.8$ s on

Fig. 2). As the injection of EtOH continued, the blue droplet started moving at an angle ~ 35° from its original position. We assumed that the actuation was a result from a decrease in surface tension arising from a limited amount of EtOH vapor dissolving in the blue droplet [31].

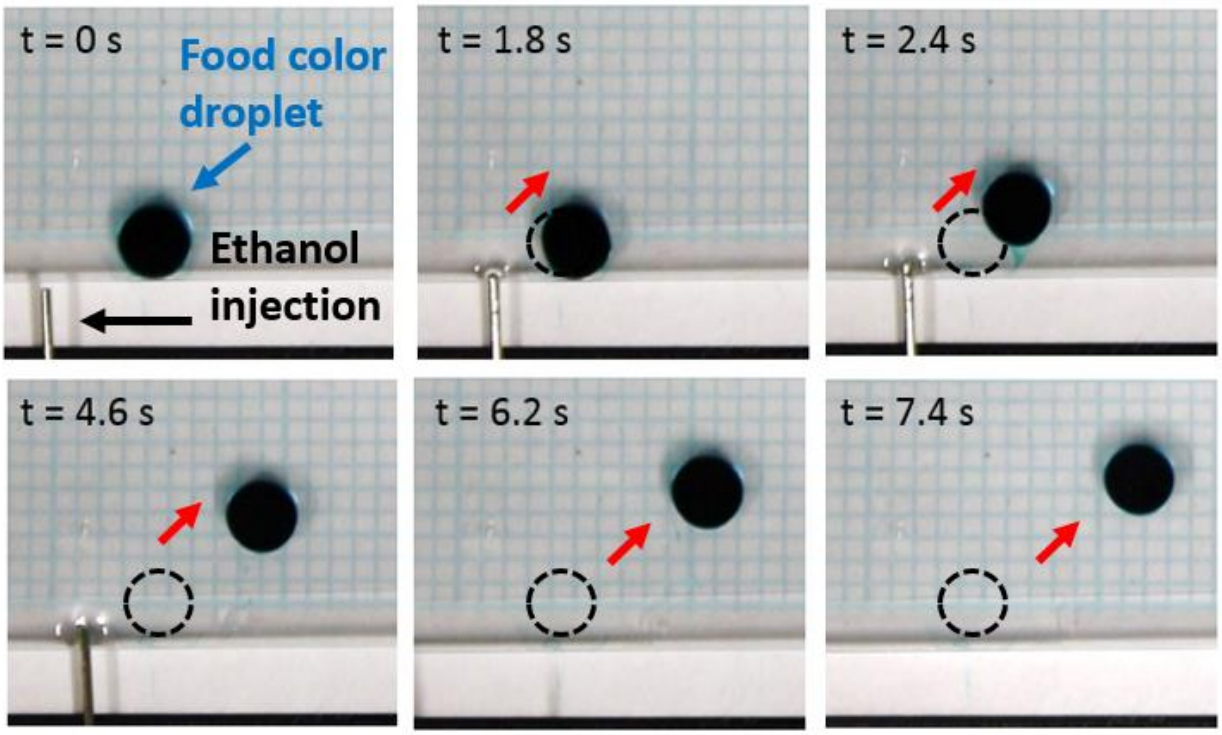

Fig. 2 Top-down photographs of the trajectory and shape morphology of a 3 μl blue food color droplet actuated by an EtOH droplet of the same volume, in a Hele-Shaw cell. Dashed circle denote initial position of droplet, pre-actuation (see video: https://youtu.be/HP8WhU1U05w).

Using Image J, the distance traveled by the blue droplet was measured by taking the center-to-center distance relative to its original position. The effects of (i) volume, and (ii) viscosity on the

distance traveled and velocity were carried out. The droplet volumes tested were 1 μl, 3 μl and 6 μl. For a cell gap height of 0.5 mm, the diameters of the droplets measured 2.33 mm, 3.33 mm, and 4.20 mm, respectively. For the viscosity study, we tested a 3 μl droplet that contained (i) water only, (ii) glycerin-to-water ratio, $C_3H_8O_3$:H_20 of 1:2, and (iii) glycerin-to-water ratio, $C_3H_8O_3$:H_20 of 1:1. The viscosities of the droplets were 8.9×10^{-4} Pa·s, 2.4×10^{-3} Pa·s, and 5.0×10^{-3} Pa·s [32], respectively.

Fig. 3(a) shows that the maximum distance traveled, as well as the time it takes to reach that distance, increases with droplet volume. A 1 μl, 3 μl and 6 μl droplet each took 20 s, 36 s and 64 s to travel to a maximum distance of 9.5 mm, 18.0 mm and 24.5 mm, respectively. A similar actuation method has been shown in our previous work, where a 1 μl droplet deposited on a 1 mm hydrophilic stripe showed a maximum traveled distance of ~ 10 mm, when actuated by an EtOH droplet of equal volume [33]. Interestingly, this distance is comparable to the distance traveled by a droplet of the same volume in this work.

Although EtOH was continually injected in the Hele-Shaw cell once the blue droplet had started moving, the velocity of the traveling droplet decreased (see Fig. 3(b)) as it moved further from the EtOH injection point. Using the difference method to obtain the velocity, followed by an exponential fit, our results show that velocity is higher for a larger droplet volume.

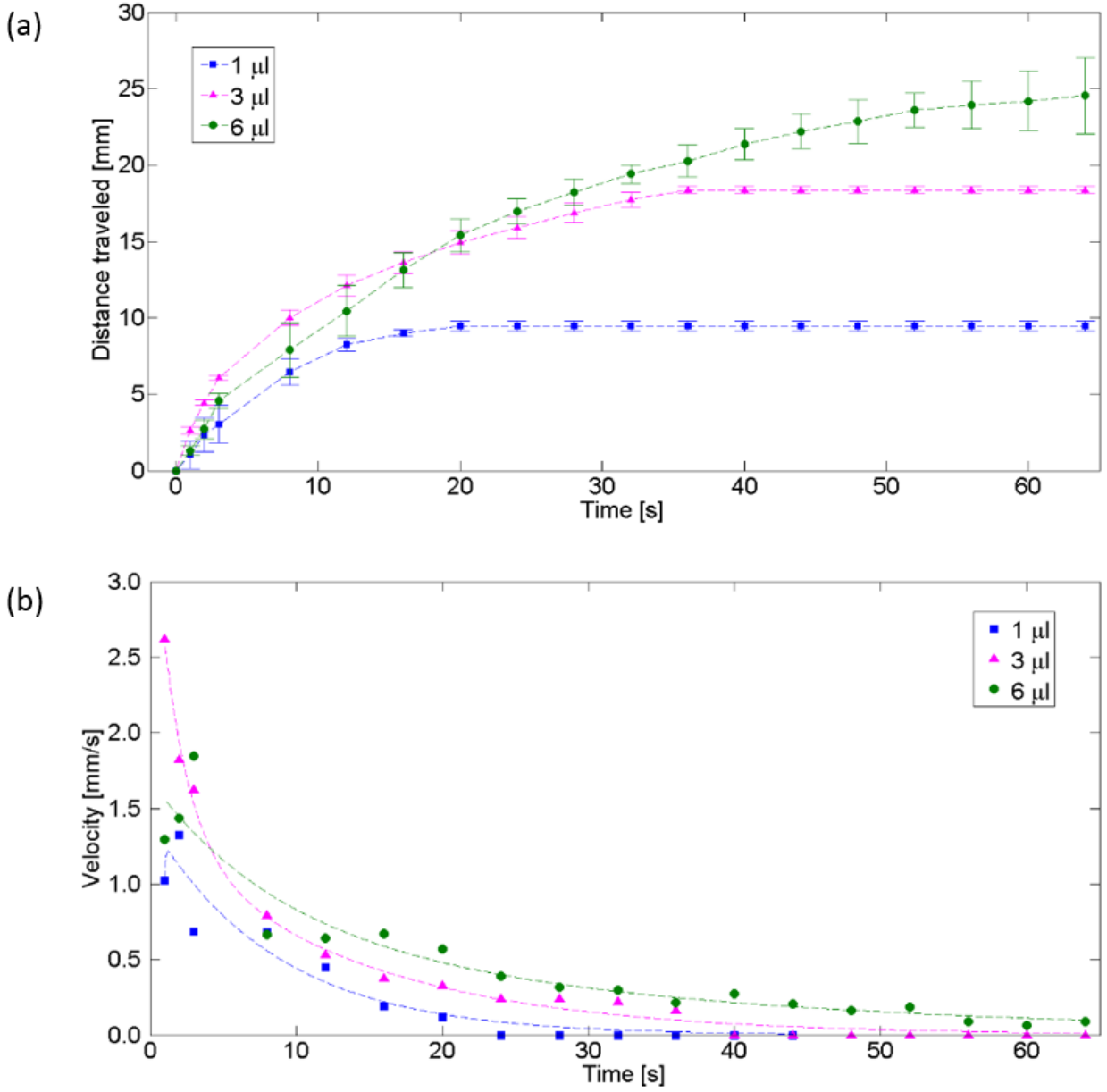

Fig. 3 The effect of droplet volume on (a) distance traveled and (b) velocity, for food color droplets actuated by EtOH in a Hele-Shaw cell. Error bars are based on three separate actuations.

For the 3 μl droplets with added glycerin, we found that the droplet with a higher glycerin concentration traveled less. As shown in Fig. 4(a), a droplet with a glycerin-to-water ratio of 1:1 traveled to a maximum distance of 10 mm in 20 s, which is lower than a 13 mm maximum distance traveled in 24 s by a droplet with a glycerin-to-water ratio of 1:2. The velocity is lower when the concentration of glycerin present in the droplet is higher (see Fig. 4(b)). Our results imply that distance and velocity are lower when viscosity is higher. Also, we found that the system was dominated by surface tension instead of viscous stresses. Using the viscosity of water, μ, velocity values of the traveling droplet, V, and the surface tension of water, σ, the capillary number, $Ca = \mu V/\sigma$ was calculated to be between 6.3 x 10^{-6} to 2.0 x 10^{-5}. Therefore, if the droplet deforms from its circular shape, surface tension will quickly bring it back to its original shape. This is evident from our experiments, where we observed only a slight ellipse at times.

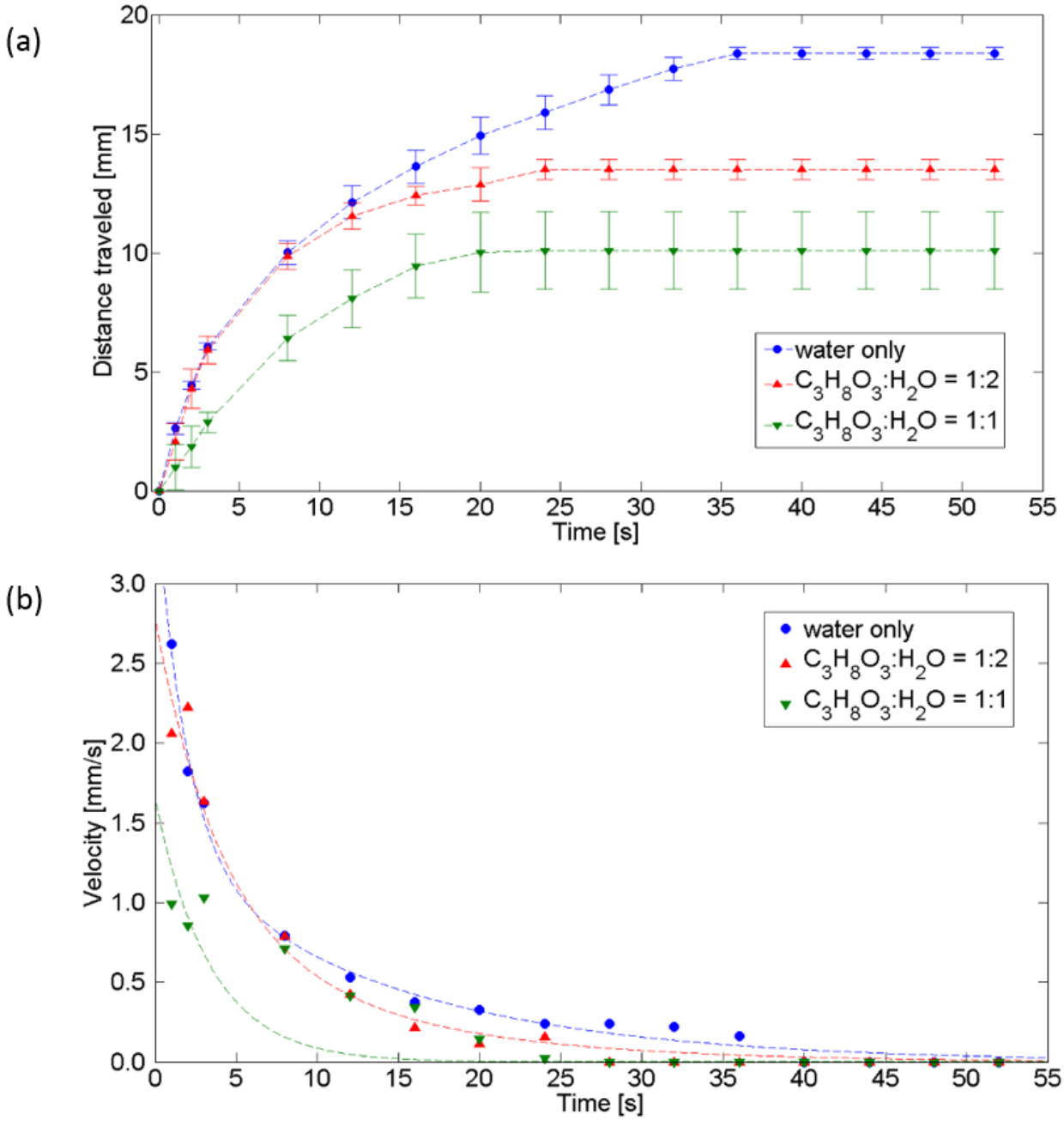

Fig. 4 The effect of viscosity on (a) distance traveled and (b) velocity, for food color droplets actuated by EtOH in a Hele-Shaw cell. Error bars are based on three separate actuations.

II. Analytical

Using experimental values in Eq. (1) to (3), the forces acting upon a 3 μl, food color-only droplet were calculated and depicted in the graphs shown in Fig. 5. Again, we used the difference method to obtain the acceleration for Fig. 5(a).

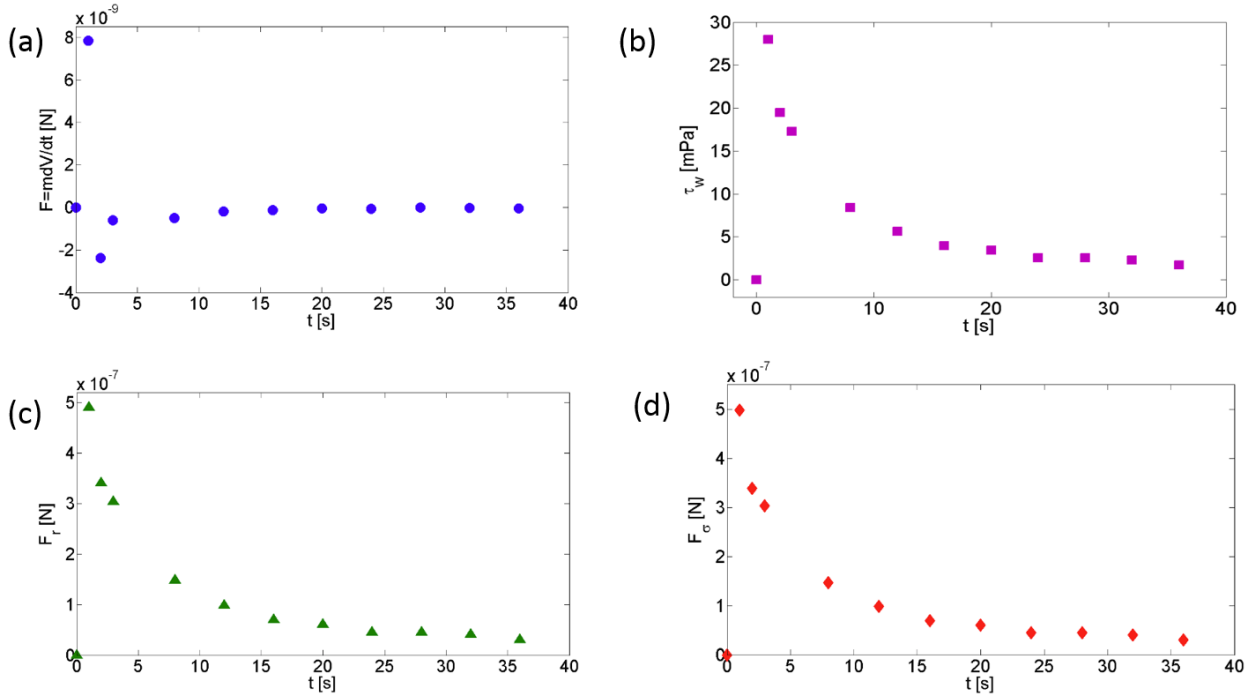

Fig. 5 Analytical values of forces acting upon a 3 μl, food color-only droplet in a Hele-Shaw cell: (a) Force as a result of traveling velocity, $F = mdV/dt$, (b) wall shear stress, τ_w, (c) viscous resistive force, F_r, and (d) Marangoni force, F_σ.

As a result of decreasing velocity that eventually reaches zero when motion stops, the forces acting upon the droplet, as expected, tends to zero as time progresses. At t = 1 s, the Marangoni force, F_σ exceeds the viscous resistive force, F_r by only 8.0 × 10^{-9} N (see Fig. 5). Nevertheless, this magnitude resulted in the actuation of the droplet, with a distance ~ 2.6 mm (see Fig. 3(a)).

We then analyzed the concentration of EtOH at positions A and B as shown in Fig. 1(b). Using $M = 2.37 \times 10^{-6}$ kg for the mass of a 3 µl EtOH, $D = 10^{-6}$ m^2/s for the typical diffusion constant value for the vapor of a volatile liquid [34] and L the experimental traveled distance, we calculated C_A and C_B by substituting $\alpha = 0$ and $\alpha = \pi$, respectively in Eq. (11). We obtained a distribution of EtOH vapor concentration on two opposing sides of the droplet as a function of time, as shown in Fig. 6. C_A was the highest initially and decays over time. Upon closer analysis, we found that the range for C_B is only ~ 5.84 × 10^{-7} g/mm^3 while the range for C_A is two orders of magnitude higher, ~ 1.68 × 10^{-5} g/mm^3. The initial rate of change of C_A is much higher than that of C_B but over time the difference in concentration, $(C_A - C_B)$ becomes smaller, suggesting a trend towards uniform concentration.

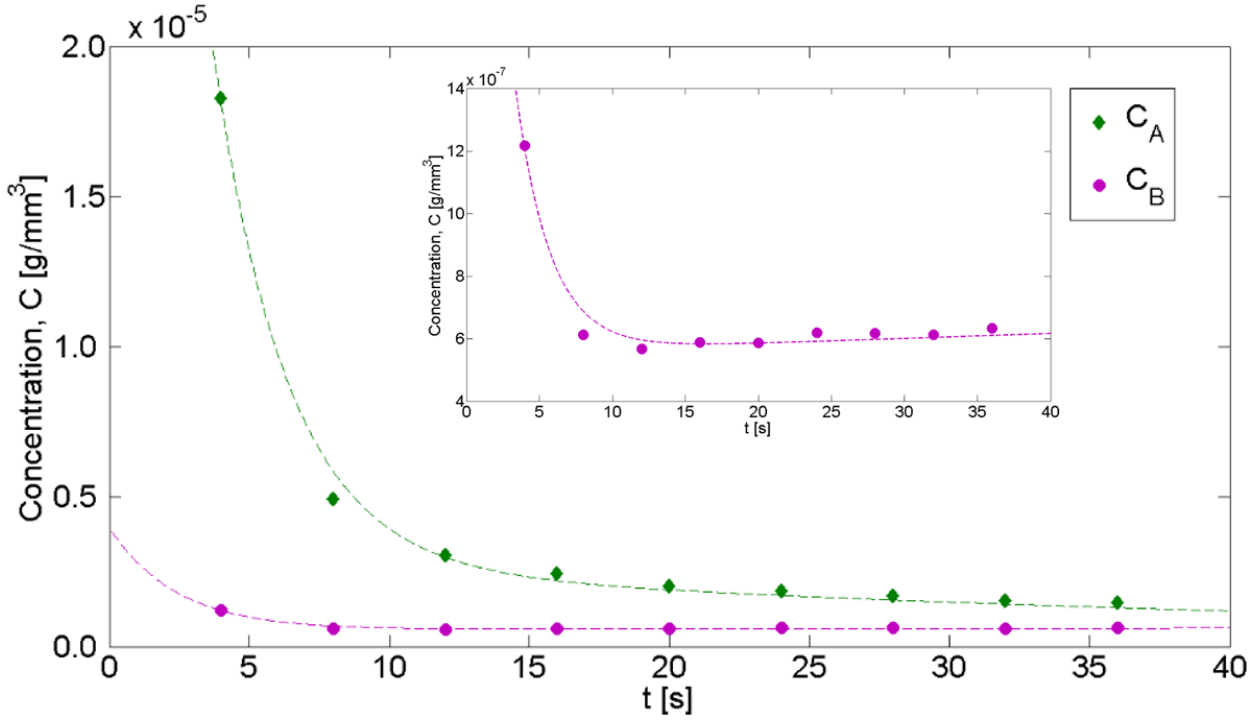

Fig. 6 Distribution of EtOH concentration on two opposing sides of a 3 μl, food color-only droplet in a Hele-Shaw cell as a function of time. Inset shows a close-up of C_B.

Additionally, by substituting the derived expressions for F_r (Eq. (4)) and F_σ (Eq. (7)) into Eq. (1), we obtain

$$m\frac{dV}{dt} = \frac{8}{3}R_o \cos\theta_c\,(\sigma_B - \sigma_A) - \frac{12\pi R_o^2 \mu V}{h}. \tag{16}$$

Solving this equation gives

$$V(t) = \frac{2h\cos\theta_c(\sigma_B - \sigma_A)}{9\pi R_o \mu}\left\{1 - e^{-\frac{12\pi R_{o\mu}^2}{hm}t}\right\}, \tag{17}$$

where the time-dependent velocity is now expressed as a function of various parameters. To study the impact of volume on surface tension difference, we rearrange Eq. (17) to obtain

$$(\sigma_B - \sigma_A) = \frac{9\pi R_o \mu}{2h\cos\theta_c}\frac{V}{\left\{1 - e^{-\frac{12\pi R_{o\mu}^2}{hm}t}\right\}}. \tag{18}$$

By varying the radius using the three experimental radii, along with experimental velocity values for a 3 μl, food color-only droplet into Eq. (18), our results show that surface tension difference diminishes sooner for a smaller droplet, as shown in Fig. 7(a). This implies that a smaller droplet would stop moving sooner, which agrees with our experimental results (see Fig. 3(a)). Next, we studied the impact of viscosity on velocity. By substituting the newly-attained surface tension difference values for a 3 μl droplet and the viscosity values from experiment into Eq. (17), we found that velocity decreases with viscosity, as shown in Fig. 7(b). This agrees with our experimental results shown in Fig. 4(b).

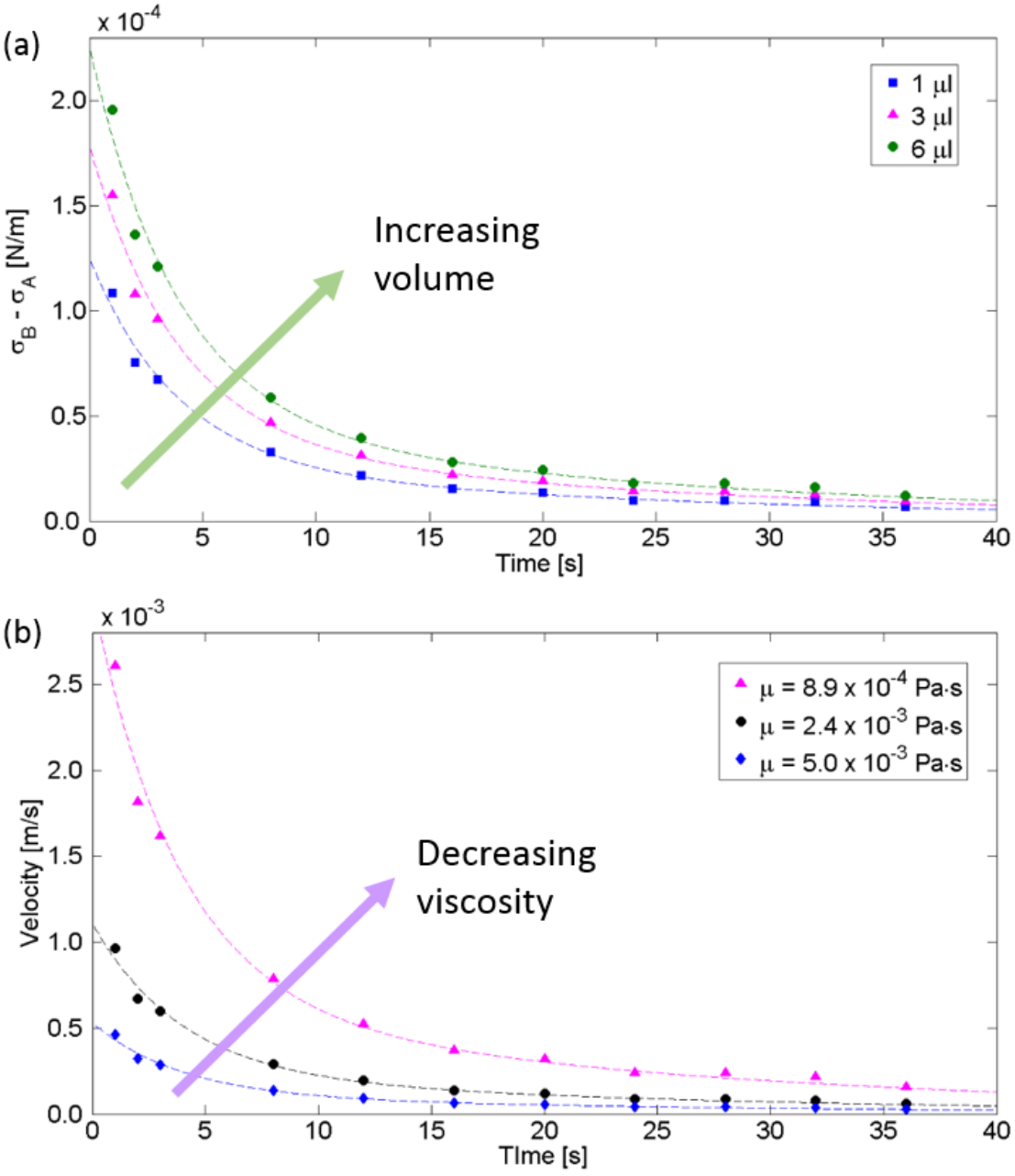

Fig. 7 The correlation between (a) surface tension difference, $(\sigma_B - \sigma_A)$ and volume, and (b) velocity and viscosity, based on the expression shown in Eq. (17).

Furthermore, we obtained the expression for distance by integrating Eq. (17). After substituting an approximate exponential fit for the surface tension difference of a 3 μl droplet, which reads

$$(\sigma_B - \sigma_A)(t) = 0.0001e^{-0.074t}, \tag{19}$$

the expression for distance is given by

$$X(t) = \frac{0.0002h\cos\theta_c}{9\pi R_o\mu}\left\{(0.074hm + 12\pi R_o^2\mu)e^{-\frac{0.074hm-12\pi R_o^2\mu}{hm}t} - 0.074e^{-0.074t}\right\}. \tag{20}$$

The impact of contact angle on distance traveled is studied using this expression. Using the values: $h = 5.0 \times 10^{-3}$ m, $R_o = 1.67 \times 10^{-3}$ m, $m = 3.0 \times 10^{-6}$ kg, $\mu = 8.9 \times 10^{-6}$ Pa·s, and varying the contact angle, θ_c, our results show that the maximum distance a droplet can travel increases as its contact angle decreases, as shown in Fig. 8.

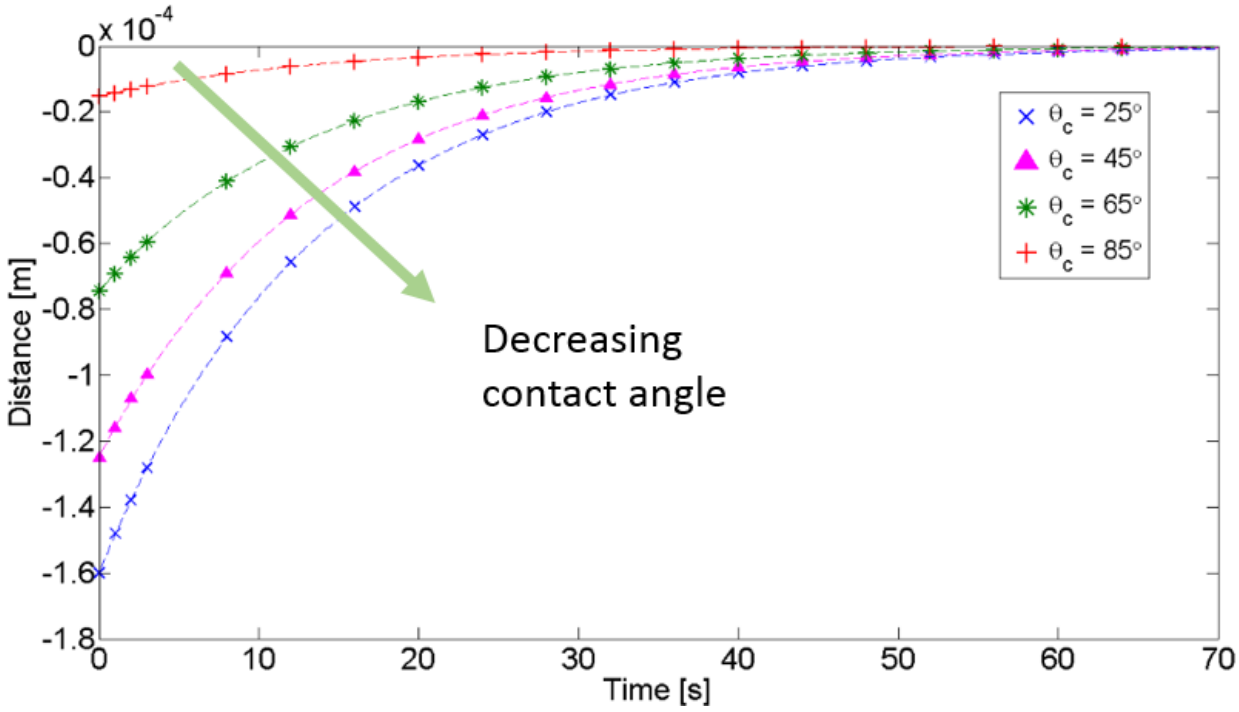

Fig. 8 The effect of contact angle on the distance traveled for a droplet in a Hele-Shaw cell.

III. Numerical

In order to estimate the viscous resistive force, F_r, we performed our simulations using body force or $\boldsymbol{F}$ values of 1, 10, 100, 400, 1000, 3000, 5000, 8000 and 10000 N/m^3, imposed in the x-direction of a 3 μl droplet, to be solved in Eq. (12). To ensure the accuracy of our simulations, we monitored the volume of the droplet, which showed mass conservation at all t. Our simulations showed that the velocity eventually saturates as a result of balanced viscous resistive force and body force in the drop and at the contact lines. Therefore, at the terminal velocity, the viscous resistive force equals the body force. A relationship between the viscous resistive force and velocity was then attained (see Fig. 9).

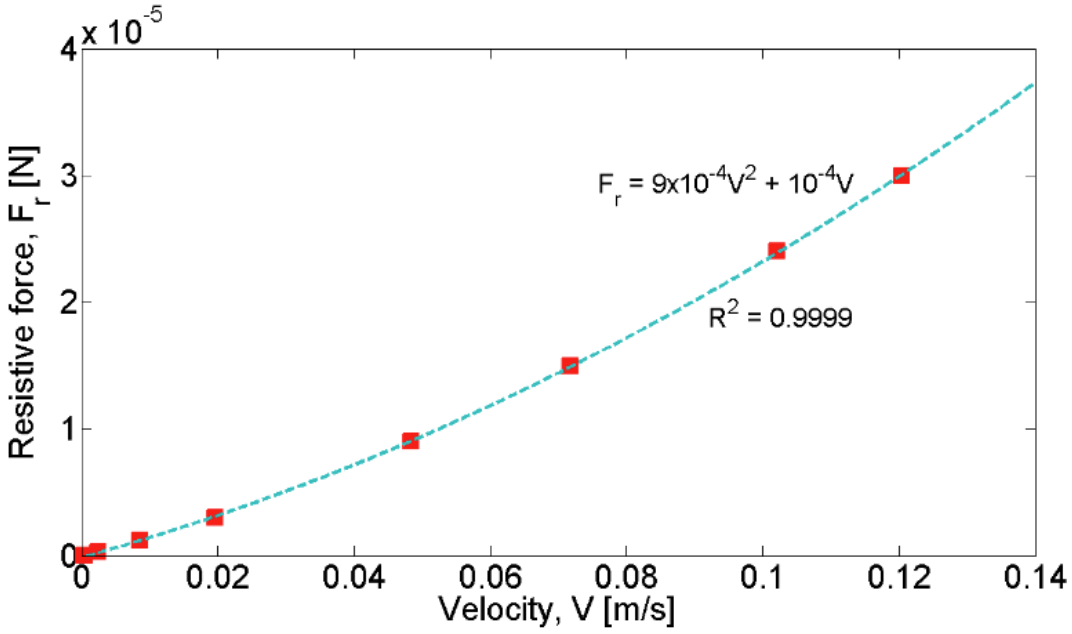

Fig. 9 Relationship between viscous resistive force and velocity attained numerically.

Through a quadratic fit, the viscous resistive force is approximated as

$$F_r = 9 \times 10^{-4} V^2 + 10^{-4} V. \tag{21}$$

Using experimental velocity values, F_r can now be calculated and substituted in Eq. (1) to obtain the Marangoni force, F_σ. The multipliers 9×10^{-4} and 10^{-4} in Eq. (21) contain units of kg/m and kg/s respectively. The trend for F_σ attained analytically and numerically are similar; however, the values at initial times do not match closely (see Fig. 10(a)).

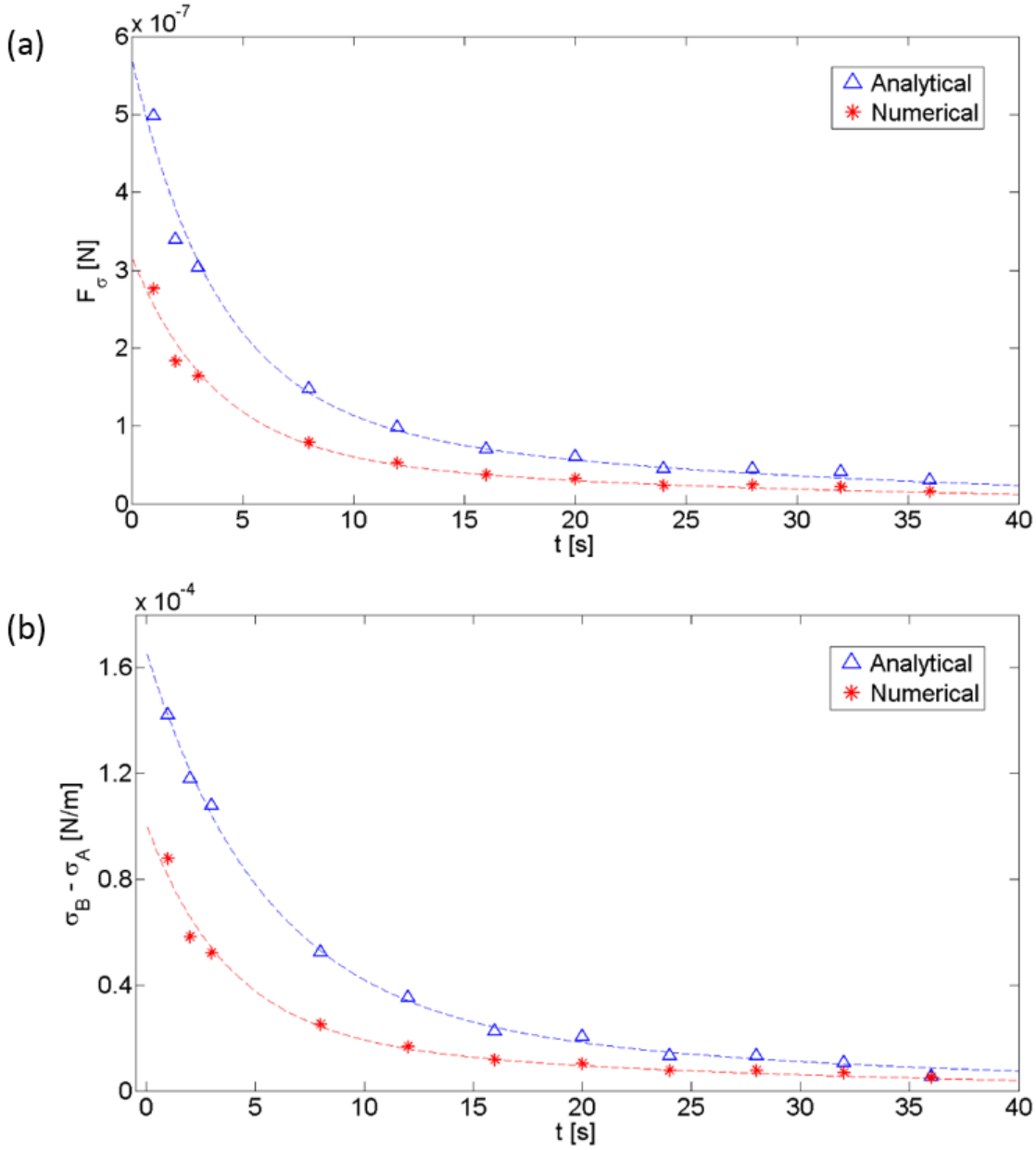

Fig. 10 Comparison of analytical and numerical values of (a) Marangoni force, F_σ and (b) surface tension difference $(\sigma_B - \sigma_A)$, obtained based on F_σ.

This could be attributed to the dissipation at the contact lines and menisci captured numerically, but was not accounted for analytically. Nevertheless, the discrepancy between numerical and analytical values is small, with an average delta of 6.97×10^{-8} N. This value corresponds to the dissipation at the menisci.

Another quantity of interest is the surface tension difference between point B and point A, as shown in Fig. 1(b). Rearranging Eq. (7), we obtain:

$$(\sigma_B - \sigma_A) = \frac{3}{8}\frac{F_\sigma}{R_o \cos\theta_c}. \tag{22}$$

Using the analytical and numerical values of F_σ (see Fig. 10(a)) in Eq. (22), we obtain a surface tension difference profile, as shown in Fig. 10(b). The initial value at t = 1 s indicate that only a small surface tension difference, i.e. 8.8×10^{-5} N/m (numerical) or 1.4×10^{-4} N/m (analytical) is required to induce motion. In addition, the surface tension of a water-ethanol mixture can be calculated using the following correlation [35]:

$$\frac{\sigma_w - \sigma(c)}{\sigma_w - \sigma_e} = \frac{1 + a(1-c)}{1 - b(1-c)}c, \tag{23}$$

where the surface tension of water, σ_w and of EtOH, σ_e are 0.072 N/m and 0.022 N/m respectively, (a,b) = (0.917, 0.956) are constants and c is the mole fraction of EtOH in the mixture [35]. First, we assume that the droplet is purely water at point B, the point farthest from the EtOH source. As

such, there is no EtOH at point B. At t = 1 s, the Marangoni force, F_σ is maximum with a value of 2.76×10^{-7} N/m attained numerically. By using the maximum F_σ and $\sigma_B = 0.072$ N/m. in Eq. (22), we obtain σ_A = 0.071912 N/m. Next, by substituting the calculated σ_A into $\sigma(c)$ of Eq. (23), we obtain an EtOH mole fraction value, c of 6.53×10^{-5}. This means that at t = 1 s, the mixture contains 0.0065% EtOH, a very small amount but sufficient to cause an actuation distance of ~ 2.6 mm in a 3 μl droplet (see Fig. 3(a)), as a result of surface tension gradient.

From the surface tension difference values, $(\sigma_B - \sigma_A)$ in Fig. 10(b), we can now obtain the angular surface tension values, $\sigma(\alpha)$ through Eq. (6). Again, by assuming that the droplet is purely water at point B ($\sigma_B = 0.072$ N/m), σ_A is calculated. The distribution of angular surface tension attained numerically is as shown in Fig. 11. It is interesting to note that at t = 4 s, the point closest to the EtOH point source at α = 0 is hardly affected by the EtOH vapor, as evident from the surface tension value that was closer to that of water. Nevertheless, propulsion had still occurred. Further analysis shows that the surface tension increases at a given angular position α, albeit very slightly, as the droplet moves further away from the EtOH point source over time (see Fig. 11). Similarly, the surface tension increases with angular position, but less so beyond t = 12 s.

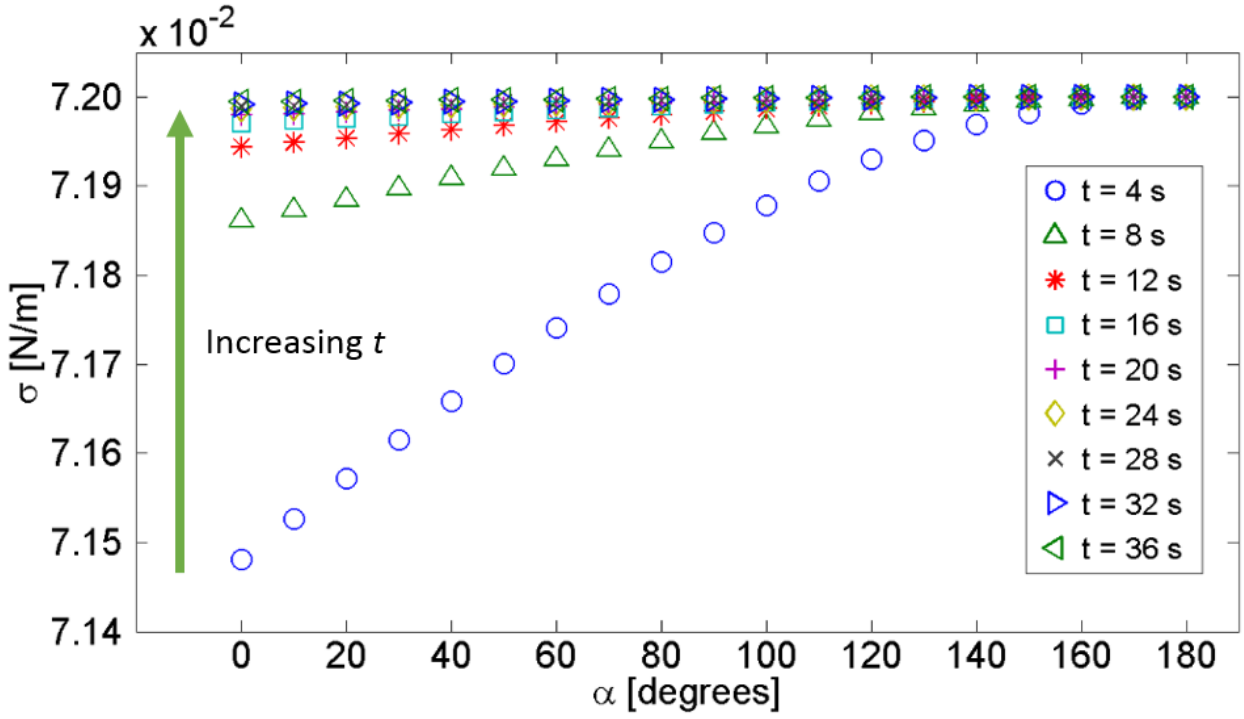

Fig. 11 Angular surface tension distribution attained numerically.

Conclusion

We have successfully demonstrated the actuation of a food color droplet with both top and bottom contact lines in a Hele-Shaw cell through surface tension gradient. By introducing an EtOH droplet next to a cylindrical food color droplet, we found that the distance traveled increases when (a) droplet volume is larger, and (b) droplet viscosity is lower. The mechanism presented in our work has yet to be reported for a cylindrical droplet in a Hele-Shaw cell, to the best of our knowledge. Another contribution of our work is in the calculation of the Marangoni force, which we could identify by generating a curve relating the viscous dissipation force to the droplet velocity. We obtained Marangoni force values that compare well against values attained analytically, thus

confirming the validity of our numerical approach. Through mathematical analysis, we found that only a small surface tension difference, between 8.8×10^{-5} N/m to 1.4×10^{-4} N/m, is required to trigger droplet motion. This suggests that only a small amount of EtOH actually crosses the droplet free surface to lower its surface tension. Consequently, this may suggest that our mechanism can be achieved using a wide range of volatile liquids. Analytically, we showed that the surface tension of the droplet increases, both with time and angular position, upon interaction with EtOH vapor. Also, we analytically showed the increase in distance traveled as contact angle decreases. Our vision for future work include controlling the motion of the sandwiched droplet by confining it to a channel, as an extension to our previous work of droplet actuation based on solutal Marangoni in an open configuration [31, 33]. This mechanism for guided passive droplet transport in an enclosed system may be applied in diagnostic portable devices, especially when the reagents under test are hazardous [20].

Acknowledgments

The authors thank Helen Devereux for her assistance, and acknowledge the financial support provided by Marsden Fund (Grant number UOC1104) administered through the Royal Society of New Zealand.

References

1. Paterson, L.: Radial fingering in a Hele Shaw cell. J. Fluid Mech. 113, 513–529 (1981)
2. Faisal, T.F., Chevalier, S., Bernabe, Y., Juanes, R., Sassi, M.: Quantitative and qualitative study of density driven CO2 mass transfer in a vertical Hele-Shaw cell. Int. J. Heat Mass Transf. 81, 901–914 (2015)
3. Wei, H.H., Waters, S.L., Liu, S.Q., Grotberg, J.B.: Flow in a wavy-walled channel lined with a poroelastic layer. J. Fluid Mech. 492, 23–45 (2003)
4. Shen, B., Leman, M., Reyssat, M., Tabeling, P.: Dynamics of a small number of droplets in microfluidic Hele–Shaw cells. Exp. Fluids. 55, 1–10 (2014)
5. Guo, X.-R., Young, W.-B.: A two-dimensional simulation model for the molded underfill process in flip chip packaging. J. Mech. Sci. Technol. 29, 2967–2974 (2015)
6. Dhanabalan, A., van Duren, J.K.J., van Hal, P.A., van Dongen, J.L.J., Janssen, R. a. J.: Synthesis and characterization of a low bandgap conjugated polymer for bulk heterojunction photovoltaic cells. Adv. Funct. Mater. 11, 255–262 (2001)
7. Shad, S., Gates, I.D., Maini, B.B.: Investigation and visualization of liquid–liquid flow in a vertically mounted Hele-Shaw cell: flow regimes, velocity and shape of droplets. Meas. Sci. Technol. 20, 114005 (2009)
8. Sullivan, M.T., Wilkins, D., Finley, E.S., Ward, T.: Gravity and capillary pressure-driven drainage in a vertical Hele-Shaw cell: Thin film deposition. Chem. Eng. Sci. 109, 147–157 (2014)
9. Eck, I.W., Siekmann, I.J.: On bubble motion in a Hele-Shaw cell, a possibility to study two-phase flows under reduced gravity. Ing.-Arch. 47, 153–168 (1978)
10. Amselem, G., Brun, P.T., Gallaire, F., Baroud, C.N.: Breaking anchored droplets in a microfluidic Hele-Shaw cell. Phys. Rev. Appl. 3, 054006 (2015)
11. Huerre, A., Theodoly, O., Leshansky, A.M., Valignat, M.-P., Cantat, I., Jullien, M.-C.: Droplets in microchannels: dynamical properties of the lubrication film. Phys. Rev. Lett. 115, 064501 (2015)
12. Brun, P.-T., Nagel, M., Gallaire, F.: Generic path for droplet relaxation in microfluidic channels. Phys. Rev. E. 88, 043009 (2013)
13. Oswald, P., Poy, G.: Droplet relaxation in Hele-Shaw geometry: Application to the measurement of the nematic-isotropic surface tension. Phys. Rev. E. 92, 062512 (2015)
14. Köllner, T., Schwarzenberger, K., Eckert, K., Boeck, T.: Solutal Marangoni convection in a Hele–Shaw geometry: Impact of orientation and gap width. Eur. Phys. J. Spec. Top. 224, 261–276 (2015)
15. Chinaud, M., Voulgaropoulos, V., Angeli, P.: Surfactant effects on the coalescence of a drop in a Hele-Shaw cell. Phys. Rev. E. 94, 033101 (2016). doi:10.1103/PhysRevE.94.033101
16. Darhuber, A.A., Troian, S.M.: Principles of Microfluidic Actuation by Modulation of Surface Stresses. Annu. Rev. Fluid Mech. 37, 425–455 (2005)
17. Gomba, J.M., Homsy, G.M.: Regimes of thermocapillary migration of droplets under partial wetting conditions. J. Fluid Mech. 647, 125–142 (2010)

18. Bratukhin, Y.K., Zuev, A.L.: Thermocapillary drift of an air bubble in a horizontal Hele-Shaw cell. Fluid Dyn. 19, 393–398 (1984)
19. Lu, H.-W., Glasner, K., Bertozzi, A.L., Kim, C.-J.: A diffuse-interface model for electrowetting drops in a Hele-Shaw cell. J. Fluid Mech. 590, 411–435 (2007)
20. Lee, J.S., Fung, Y.C.: Stokes flow around a circular cylindrical post confined between two parallel plates. J. Fluid Mech. 37, 657–670 (1969)
21. Gallaire, F., Meliga, P., Laure, P., Baroud, C.N.: Marangoni induced force on a drop in a Hele Shaw cell. Phys. Fluids 1994-Present. 26, 062105 (2014)
22. Abbyad, P., Dangla, R., Alexandrou, A., Baroud, C.N.: Rails and anchors: guiding and trapping droplet microreactors in two dimensions. Lab. Chip. 11, 813–821 (2011)
23. Huebner, A., Bratton, D., Whyte, G., Yang, M., Abell, C., Hollfelder, F., others: Static microdroplet arrays: a microfluidic device for droplet trapping, incubation and release for enzymatic and cell-based assays. Lab. Chip. 9, 692–698 (2009)
24. Song, H., Ismagilov, R.F.: Millisecond kinetics on a microfluidic chip using nanoliters of reagents. J. Am. Chem. Soc. 125, 14613–14619 (2003)
25. Yobas, L., Cheow, L.F., Tang, K.-C., Yong, S.-E., Ong, E.K.-Z., Wong, L., Teo, W.C.-Y., Ji, H., Rafeah, S., Yu, C.: A self-contained fully-enclosed microfluidic cartridge for lab on a chip. Biomed. Microdevices. 11, 1279–1288 (2009)
26. Rasband, W.S.: Image J, http://www.imagej.nih.gov/ij/
27. Ahmed, G., Sellier, M., Jermy, M., Taylor, M.: Modeling the effects of contact angle hysteresis on the sliding of droplets down inclined surfaces. Eur. J. Mech. - B Fluids. 48, 218–230 (2014)
28. http://web.mit.edu/1.061/www/dream/THREE/THREETHEORY.PDF.
29. Bico, J., Quéré, D.: Falling Slugs. J. Colloid Interface Sci. 243, 262–264 (2001)
30. Karpitschka, S., Pandey, A., Lubbers, L.A., Weijs, J.H., Botto, L., Das, S., Andreotti, B., Snoeijer, J.H.: Liquid drops attract or repel by the inverted Cheerios effect. Proc. Natl. Acad. Sci. 113, 7403–7407 (2016)
31. Sellier, M., Nock, V., Gaubert, C., Verdier, C.: Droplet actuation induced by coalescence: Experimental evidences and phenomenological modeling. Eur. Phys. J. Spec. Top. 219, 131–141 (2013)
32. Sheely, M.L.: Glycerol viscosity tables. Ind. Eng. Chem. 24, 1060–1064 (1932)
33. Ng, V.-V., Sellier, M., Nock, V.: Marangoni-induced actuation of miscible liquid droplets on an incline. Int. J. Multiph. Flow. 82, 27–34 (2016)
34. Sultan, E., Boudaoud, A., Amar, M.B.: Evaporation of a thin film: diffusion of the vapour and Marangoni instabilities. J. Fluid Mech. 543, 183–202 (2005)
35. Vazquez, G., Alvarez, E., Navaza, J.M.: Surface Tension of Alcohol Water + Water from 20 to 50 degree C. J. Chem. Eng. Data. 40, 611–614 (1995)